HHS Public Access

Author manuscript

Magn Reson Med. Author manuscript; available in PMC 2017 July 18.

Published in final edited form as:

Magn Reson Med. 2017 March ; 77(3): 1142–1150. doi:10.1002/mrm.26201.

Whole-Brain Intracranial Vessel Wall Imaging at 3 Tesla Using Cerebrospinal Fluid–Attenuated T1-Weighted 3D Turbo Spin Echo

Zhaoyang Fan[1,†,*], **Qi Yang**[1,2,†], **Zixin Deng**[1,3], **Yuxia Li**[4], **Xiaoming Bi**[5], **Shlee Song**[6], and **Debiao Li**[1,3]

[1]Biomedical Imaging Research Institute, Department of Biomedical Sciences, Cedars-Sinai Medical Center, Los Angeles, California, USA

[2]Department of Radiology, Xuanwu Hospital, Beijing, China

[3]Department of Bioengineering, University of California, Los Angeles, California, USA

[4]Department of Neurology, Xuanwu Hospital, Beijing, China

[5]MR R&D, Siemens Healthcare, Los Angeles, California, USA

[6]Department of Neurology, Cedars-Sinai Medical Center, Los Angeles, California, USA

Abstract

Purpose—Although three-dimensional (3D) turbo spin echo (TSE) with variable flip angles has proven to be useful for intracranial vessel wall imaging, it is associated with inadequate suppression of cerebrospinal fluid (CSF) signals and limited spatial coverage at 3 Tesla (T). This work aimed to modify the sequence and develop a protocol to achieve whole-brain, CSF-attenuated T_1-weighted vessel wall imaging.

Methods—Nonselective excitation and a flip-down radiofrequency pulse module were incorporated into a commercial 3D TSE sequence. A protocol based on the sequence was designed to achieve T_1-weighted vessel wall imaging with whole-brain spatial coverage, enhanced CSF-signal suppression, and isotropic 0.5-mm resolution. Human volunteer and pilot patient studies were performed to qualitatively and quantitatively demonstrate the advantages of the sequence.

Results—Compared with the original sequence, the modified sequence significantly improved the T_1-weighted image contrast score (2.07 ± 0.19 versus 3.00 ± 0.00, $P = 0.011$), vessel wall-to-CSF contrast ratio (0.14 ± 0.16 versus 0.52 ± 0.30, $P = 0.007$) and contrast-to-noise ratio (1.69 ± 2.18 versus 4.26 ± 2.30, $P = 0.022$). Significant improvement in vessel wall outer boundary sharpness was observed in several major arterial segments.

Conclusions—The new 3D TSE sequence allows for high-quality T_1-weighted intracranial vessel wall imaging at 3 T. It may potentially aid in depicting small arteries and revealing T_1-mediated high-signal wall abnormalities.

[*]Correspondence to: Zhaoyang Fan, Ph.D., Biomedical Imaging Research Institute, Cedars-Sinai Medical Center, 8700 Beverly Blvd., PACT 800, Los Angeles, CA 90048. Telephone: (310) 425-9814; fanzhaoyang@gmail.com.

[†]These authors contributed equally to this work.

Keywords

intracranial vessel wall; stroke; cerebral arteries; magnetic resonance imaging; vessel wall imaging

INTRODUCTION

Stroke is a leading cause of mortality and morbidity worldwide and arises from different intracranial wall pathologies, such as atherosclerosis, vasculitis, and Moyamoya disease (1). Accurate characterization of these pathologies may help elucidate stroke etiology and allow for therapeutic intervention before severe cerebrovascular events occur (2). Conventional lumenography-based imaging methods do not provide information about the pathologic processes of the vessel wall (3,4). In contrast, high-resolution black-blood MR imaging permits direct assessment of the intracranial vessel wall (5–7).

Intracranial vessel wall MR imaging is technically demanding, given the smaller size and relatively deep location (8). Two-dimensional (2D) turbo spin-echo (TSE) sequences have previously been used to ensure high in-plane spatial resolution and adequate signal-to-noise ratio (SNR) from deep vessels (5–7). Recently, three-dimensional (3D) TSE with variable refocusing flip angles is drawing attention because of distinct advantages over its 2D counterpart in time efficiency, spatial coverage, SNR, and spatial resolution isotropy (9).

T_1-weighted 3D TSE, in particular, is of great interest because of the ability to reveal vessel wall abnormalities that exhibit high signal intensity with or without the use of contrast media, such as intraplaque hemorrhage, wall inflammation, and dissection hematoma (10–13). Despite promising results previously demonstrated at 1.5 or 3 Tesla (T), the technique has two major limitations. First, inadequate suppression of cerebrospinal fluid (CSF) signals renders it difficult to discern the outer boundary of the vessel wall, making, for example, positive wall remodeling undetectable. Second, spatial coverage is usually limited to a thin target volume in all current imaging protocols because of the conflicting demands on scan times, SNR, and desired spatial resolution. For example, Qiao et al recently presented a protocol that employed a 45-mm-thick oblique coronal slab to cover only major intracranial arterial segments with isotropic 0.5-mm spatial resolution within 7.9 min (9). Hence, culprit lesions at some arterial branches might be missed. Simply expanding the spatial coverage to the whole brain without optimizing their protocols would require a scan time of over 15 min. To address these issues, van der Kolk et al proposed a CSF-attenuated 3D TSE sequence that leveraged a higher field strength, 7T, to achieve whole-brain intracranial vessel wall imaging with sufficient SNR and isotropic 0.8-mm spatial resolution; a reasonable scan time of 11 min was possible with an acceleration rate of 6 (14). However, such an acceleration rate cannot be achieved at clinically available, lower field strengths with standard hardware.

The aim of this work was to improve the 3D TSE sequence commercially available at 3T and develop a T_1-weighted intracranial vessel wall imaging protocol that offers whole-brain spatial coverage, CSF attenuation, and isotropic 0.5-mm spatial resolution within a reasonable scan time. Human volunteer and pilot patient studies were performed to demonstrate the feasibility and advantages of the new technique.

METHODS

MR Sequence Design

Modifications were performed on the basis of a commercial 3D variable-flip-angle TSE sequence, namely SPACE (Sampling Perfection with Application optimized Contrast using different flip angle Evolution) (15). Figure 1a illustrates the diagram of our modified sequence. To enable whole-brain spatial coverage, a nonselective, hard radiofrequency (RF) pulse is used for excitation. The short-duration pulse allowed the echo time (TE) to reduce from 20 to 10 ms, which helps to increase both the T_1 weighting and SNR. A method previously proposed for optimal T_1-weighted brain tissue imaging is adopted to suppress signals from the CSF (16). Specifically, a flip-down RF pulse module based on a signal restore scheme is applied immediately after each refocusing pulse train. At the end of the pulse train, CSF has a considerable amount of magnetization remaining, not only along the longitudinal (z) axis, but also in the transverse plane, because of its substantially long T_2. In contrast to a simple nonselective inversion pulse, this module uses three RF pulses to transfer all magnetization to the z-axis. This makes CSF's longitudinal magnetization more negative immediately before subsequent inversion recovery (IR), which facilitates its signal attenuation. The new sequence is therefore referred to as IR-SPACE throughout the manuscript. Nonselective saturation is applied at the beginning of the pulse sequence to achieve quick transition of magnetizations to a steady state. To reduce the scan time, minimal phase and partition-encoding steps are desired. Thus, a sagittal-orientated imaging volume is prescribed that requires fewer partitions than other imaging orientations when covering the head and part of the neck; meanwhile, three 35–40-mm spatial presaturation bands located next to the imaging volume are applied immediately before excitation to suppress the signals from the out-of-volume nose and ears (Fig. 1b). Suppressing free-induction-decay artifacts using multiple signal averages is not needed with the whole-brain spatial coverage (15); therefore, one signal average can be used to minimize the scan time.

Study Population

Seven volunteers (4 females; age range 32–65 years; mean age 46 years) without known cerebrovascular disease were recruited in a volunteer study. In addition, as a pilot study, four patients who were known to have severe luminal stenosis as a result of atherosclerosis (1 female and 2 males, mean age 57 years) or lupus (a 37-year-old female) disease were recruited. Both studies were approved by the local institutional review board, and written, informed consent was obtained from the subjects before MR imaging.

MR Imaging

Imaging was performed on a 3T whole-body MR system (MAGNETOM Verio; Siemens Healthcare, Erlangen, Germany) equipped with a 32-channel head coil (Siemens Healthcare). Before vessel wall imaging, 3D time-of-flight (TOF) MR angiography was acquired with spatial resolution of $0.52\times0.52\times0.52$ mm^3 (with slice interpolation) and used as a reference for assessing vessel wall images whenever necessary.

To demonstrate the feasibility and advantages of IR-SPACE, two scans (SPACE and IR-SPACE, respectively) were then conducted in a random order in volunteers. The major

imaging parameters shared by the two sequences were 3D sagittal orientation; TR/TE=800/10 ms; field of view=180×200×(108–116) mm^3; matrix size = 346×384×(208–224) with 7.1–7.7% partition oversampling; spatial resolution = 0.52×0.52×0.52 mm^3 without interpolation; 6/8 partial Fourier in the partition-encoding direction; parallel imaging (GRAPPA) acceleration rate = 2 in the phase-encoding direction; signal average = 1; scan time = 11 min 14 s–12 min. A turbo factor of 37 was chosen as a trade-off among adequate signal intensity, sufficient T_1 weighting, and short scan times. The inversion time for IR-SPACE was 600 ms.

To ascertain whether the image quality of the new sequence is acceptable in the postcontrast state, an IR-SPACE scan was repeated in three of the seven subjects 5 min after injection of 0.1 mmol/kg body weight Gadoversetamide (OptiMark; Mallinckrodt, Hazelwood, Missouri) and 20 mL saline.

Moreover, a pilot study of four clinical patients was performed to preliminarily evaluate the diagnostic usefulness and subject tolerance. Because of the time constraints in clinical settings, patients underwent only pre- and postcontrast IR-SPACE scans using the described protocol.

Image Analysis

All 3D images were loaded to a workstation (Syngo MultiModality Workplace; Siemens Healthcare, Germany) for image processing and viewing. For volunteer images, 2D cross-sectional images of 0.52 mm thickness were first reconstructed by an experienced neuroradiologist (Q. Y.) from individual precontrast 3D image sets using multiplanar reformatting for each of arterial segments, including the distal basilar artery (BA), the internal carotid artery supraclinoid segment (ICA C4), the middle cerebral artery (MCA) M1–M3 segments, the anterior cerebral artery (ACA) A1 and A2 segments, and the posterior cerebral artery (PCA) P1 and P2 segments from an arbitrarily selected side. Care was taken to ensure location match between SPACE and IR-SPACE scans. The original 3D and reformatted 2D images then underwent the following analyses.

1. Qualitative Analyses—Precontrast SPACE and IR-SPACE images were randomized and presented to two readers (one neuroradiologist [Q. Y.] with 10 years of experience and one MR physicist (Z. F.) with 8 years of experience in MR vessel wall imaging), who were blinded to the subject and sequence information. Overall T_1-weighted image contrast was graded by readers in consensus for each 3D image set on a 4-point scale (0: poor; 3: excellent). Using reformatted 2D images, vessel wall delineation was graded by readers independently (to allow for the assessment of interreader agreement with large-size samples) for each of arterial segments on a 4-point scale: 0 denotes that ≤ 50% of the vessel wall is visible, 1 denotes that > 50% of the vessel wall is visible, 2 denotes that the vessel wall is delineated with adequate signal and contrast to the lumen and CSF, and 3 denotes that the vessel wall is delineated with excellent SNR and sharp contrast to the lumen and CSF. Additionally, vessel wall delineation on postcontrast IR-SPACE images was scored by readers in consensus.

2. Quantitative Analyses—The reconstructed ICA C4 cross-sectional images were magnified four times through bilinear interpolation. To evaluate the contrast gain and loss when using IR-SPACE versus SPACE, mean signal intensity (S) was measured from the vessel wall of ICA C4, adjacent vessel lumen, CSF, white matter (WM), and gray matter (GM) using region-of-interest (ROI) analysis. ROIs were manually prescribed on IR-SPACE images and then propagated to the corresponding SPACE images, assuming that the former allowed for easier identification of wall outer boundary, and WM and GM. The contrast ratios (CR = [S1–S2]/S2) between WM and GM, between the vessel wall and surrounding CSF, and between the vessel wall and lumen were respectively calculated. The wall-to-CSF contrast-to-noise ratio (CNR) was also determined as $(S_{wall}-S_{CSF})/\sigma$, in which σ is the noise measured as signal standard deviation from an artifact-free air region (ROI area > 200 mm^2) of the sphenoid sinus cavity in close proximity to the selected ICA C4 segment. In addition, the sharpness at the outer wall boundary was measured using an in-house MATLAB (v. R2013a; MathWorks, Natick, Massachusetts) program for BA, ICA C4, MCA M1-M3, ACA A1 and A2, and PCA P1 and P2, respectively, according to a previous method (17).

Whole-brain vessel wall images from patients underwent a diagnostic evaluation by the same neuroradiologist who was blinded to the subject identity and images from the other sequences.

Statistical Analysis

Statistical tests were performed using Stata (version 10.0; StataCorp LP, College Station, Texas). A paired two-tailed Wilcoxon signed rank test was used for the comparison of ordinal image scores (ie, consensus scores on overall T_1-weighted image contrast and averaged scores on vessel wall delineation) between IR-SPACE and SPACE. Interreader agreement in the assessment of vessel wall delineation was determined based on all evaluated segments by using a weighted Cohen's kappa test before the two readers' scores were averaged. A paired two-tailed Student's t-test was used for the comparison of CR, wall-to-CSF CNR, and sharpness. Statistical significance was defined as $P < 0.05$. Data were presented as mean ± standard deviation.

RESULTS

Volunteer Study

1. Qualitative Analyses—The new sequence and protocol setting provided complete spatial coverage for the entire intracranial arterial system. Besides the arterial segments commonly depicted by literature at 3T, smaller arterial segments such as the M3 and M4 segments of MCA, the A1 and A2 segments of ACA, and the P1 and P2 segments of PCA were all visible (Fig. 2). Compared with original SPACE, significantly improved overall T_1-weighted image contrast scores were obtained with IR-SPACE (2.07 ± 0.19 versus 3.00 ± 0.00, $P = 0.011$). Interreader agreement in the assessment of vessel wall delineation was excellent for both SPACE (weighted $\kappa = 0.87$) and IR-SPACE (weighted $\kappa = 0.90$) scans. Sharp contrast between the outer vessel wall boundary and surrounding CSF was observed at each of the major intracranial arterial segments with IR-SPACE (Figs. 2–4). In contrast, the use of IR preparation elicited slight signal dropout in the vessel wall, which, in some cases,

undermined the readers' wall delineation scores. Hence, vessel wall delineation was significantly improved (2.63 ± 0.49 versus 2.81 ± 0.43, $P = 0.01$) when all segments were assessed together, but the statistical significance was not reached when segments were individually assessed (Table 1).

2. Quantitative Analyses—Compared with original SPACE, the CR of WM to GM was significantly increased with IR-SPACE (0.16 ± 0.07 versus 0.22 ± 0.06, $P < 0.001$). As a result of the IR preparation, the vessel wall-to-lumen CR was reduced (6.83 ± 1.99 versus 4.58 ± 1.56, $P = 0.002$), but the CR of the vessel wall to surrounding CSF was significantly enhanced (0.14 ± 0.16 versus 0.52 ± 0.30, $P = 0.007$). Wall-to-CSF CNR demonstrated a similar improvement (1.69 ± 2.18 versus 4.26 ± 2.30, $P = 0.022$). Moreover, vessel-wall sharpness was significantly improved using IR-SPACE when all segments were assessed together and when ICA C4, MCA M1, M2, and M3 were assessed individually (Table 1). The basilar artery, ACA A1 and A2, and PCA P1 and P2 showed little improvement with IR-SPACE without statistical significance.

Incidental findings in the precontrast scans were reported in three of the seven volunteers by the neuroradiologist. Two of them (aged 50 and 58 years) exhibited wall thickening with relatively high signal at the MCA and ICA C4, respectively, on both SPACE and IR-SPACE images, as exemplified in Figure 3. The third one (aged 65 years) had a mild stenosis at the MCA demonstrated in both scans, but exhibited wall thickening and relatively high signal only on IR-SPACE images (Fig. 4).

Among the three subjects who received contrast medium, eccentric postcontrast enhancement was observed in the volunteer (aged 50 years) who also showed relatively high signal at the same location in the precontrast state (Fig. 3). All postcontrast scans with IR-SPACE provided acceptable image quality and vessel wall delineation (score ≥ 2).

Patient Study

IR-SPACE imaging was performed successfully in all four patients. In the three patients with atherosclerosis, a severe stenosis with eccentric wall contrast enhancement was observed with IR-SPACE, as exemplified in Figure 5. In the patient with lupus disease, severe luminal constriction with concentric wall thickening and contrast enhancement was observed at the MCA with IR-SPACE (Fig. 6). In contrast, TOF MR angiography simply revealed luminal stenosis in all cases.

DISCUSSION

In this work we developed a whole-brain T_1-weighted intracranial vessel wall imaging technique at 3 T. The technique features large spatial coverage, high and isotropic spatial resolution, and more importantly, remarkable suppression of CSF and enhanced T_1 contrast weighting. Our preliminary results suggest its great potential as a clinical tool for the assessment of vessel wall abnormalities.

In intracranial vessel wall imaging, both the isotropic, high spatial resolution and large spatial coverage are important for widespread application of an MR sequence in clinical

practice. Voxel isotropy achieved in this work provides great flexibility for wall visualization of tortuous intracranial arteries, as images can be reformatted from an arbitrary plane without losing resolution. Furthermore, an acquired high spatial resolution of 0.5 mm further aids in the assessment of small wall lesions. Most importantly, whole-brain coverage enables visualization of not only large intracranial arteries but also small arteries that may account for cerebrovascular disease, but otherwise not easily be visualized using existing limited-coverage sequences. To the best of our knowledge, this is the first work demonstrating the feasibility of using a 3D TSE-based technique to achieve isotropic 0.5-mm resolution whole-brain vessel wall imaging at 3 T.

Attenuation of signals from surrounding CSF is desirable for improving the conspicuity of the intracranial vessel wall. Because of its long T1, CSF is typically of lower signal intensity than other tissues, including the vessel wall, on T_1-weighted images acquired by commercial 3D TSE sequences. However, our experience and literature suggest that the wall-to-CSF contrast generated by this means is inadequate, leading to suboptimal visualization of the outer wall boundary (9–12). Several solutions have recently been proposed. Working at 7T, Van der Kolk et al presented a magnetization preparation inversion recovery (MPIR) method to suppress the signal from CSF (18). A long inversion time and TR are both needed for adequate CSF attenuation because of slow inversion recovery of CSF magnetization. To reduce the signal penalty on the vessel wall due to inversion preparation, a long-duration T_2 preparation module immediately applied before the inversion pulse is also needed to essentially saturate the signal from the vessel wall that will in turn undergo saturation recovery instead of inversion recovery. Another technique exploits the flow nature of CSF and uses a flow-sensitive module, ie, delay alternating with nutation for tailored excitation (DANTE), to attenuate CSF (19). However, because of certain variability of CSF velocity within the brain and between subjects, reliable CSF attenuation could be challenging. In this work, we adopted an inversion recovery–based methodology for CSF attenuation, which is a flow-independent approach similar to the MPIR method. However, T_2 preparation and long inversion time are not needed, because CSF's T_1 is much shorter at 3 T. The signal of the vessel wall appeared adequate at 3 T, likely because of its faster T_1 recovery than at 7 T, and lower acquisition acceleration rate (2 versus 6). Despite the slight sacrifice in wall signal resulting from the inversion preparation, wall-CSF contrast and sharpness of the outer wall boundary can be significantly improved, which would be beneficial for the visualization of the wall and quantification of lesion size.

The T_1 weighting of the new SPACE-based sequence is enhanced with several approaches in this work. First, the use of a short-duration hard pulse for nonselective excitation substantially reduces the echo spacing of the first spin echo, and thus the achievable TE. In contrast, the TEs used in several previous work at 3 T were approximately 20 ms or longer because of the slab-selective excitation (10–12). Second, the inversion restore module imparts strong T_1 weighting that is a distinct difference between SPACE an IR-SPACE images in this work. Compared with a simple hard inversion pulse that is usually available in commercial sequences, this module is theoretically more effective in generating T_1 weighting (16). Third, the relatively short TR and echo train length are further in favor of T_1 weighting. With the boosted T_1 weighting along with the suppression of CSF signals, we incidentally identified a precontrast high-signal feature as well as wall thickening in one

case (Fig. 4) that was missed by the non-IR SPACE scan. In addition, IR-SPACE appeared to work for postcontrast imaging, in which patients exhibited wall contrast enhancement. Based on our preliminary results, it is anticipated that the developed technique is highly suited for the detection of T_1-mediated high-signal wall abnormalities such as intraplaque hemorrhage, wall inflammation, and dissection hematoma.

There are limitations in this work. Because of the time constraints in clinical settings, direct comparison between SPACE and IR-SPACE was not performed in patients, which could otherwise help to further demonstrate the advantage of enhanced T_1 weighting in identification of high-signal abnormalities. Large-scale clinical validation on this aspect is warranted in the future. In addition, the scan time of 11–12 min is still relatively long, although this was tolerable in our studies and other work at 7 T (14,18). Motion artifacts may arise for patients who may be unable to hold still. Because of this limitation, spatial resolution of higher than 0.5 mm was not attempted in this work that could otherwise allow for the investigation of possibly visualizing even smaller arteries, such as anterior or posterior communication arteries. This issue could be overcome by either further optimization of the imaging parameters or the application of more advanced receiver coil associated with a higher imaging acceleration rate.

In conclusion, T_1-weighted IR-SPACE is a 3D black-blood and CSF-attenuated sequence allowing for whole-brain, isotropic high-spatial-resolution intracranial arterial wall imaging at 3 T. This technique has great potential to be used for the investigation of stroke etiology.

Acknowledgments

American Heart Association; Grant number: 15SDG25710441; Grant sponsor: National Institutes of Health; Grant number: NHLBI 2R01HL096119; Grant sponsor: National Science Foundation of China; Grant numbers: 81322022; 81325007; Grant sponsor: New Century Excellent Talents in University; Grant number: 13-0918.

References

1. Go AS, Mozaffarian D, Roger VL, et al. Heart disease and stroke statistics—2014 update: a report from the American Heart Association. Circulation. 2014; 129:e28–e292. [PubMed: 24352519]
2. Arenillas JF. Intracranial atherosclerosis: current concepts. Stroke. 2011; 42:S20–S23. [PubMed: 21164126]
3. Kramer CM, Anderson JD. MRI of atherosclerosis: diagnosis and monitoring therapy. Expert Rev Cardiovasc Ther. 2007; 5:69–80. [PubMed: 17187458]
4. Naghavi M, Libby P, Falk E, et al. From vulnerable plaque to vulnerable patient: a call for new definitions and risk assessment strategies: part I. Circulation. 2003; 108:1664–1672. [PubMed: 14530185]
5. Swartz RH, Bhuta SS, Farb RI, et al. Intracranial arterial wall imaging using high-resolution 3-tesla contrast-enhanced MRI. Neurology. 2009; 72:627–634. [PubMed: 19221296]
6. Xu W-H, Li M-L, Gao S, Ni J, Zhou L-X, Yao M, Peng Bin, Feng F, Jin Z-Y, Cui L-Y. Atherosclerosis. Atherosclerosis. 2010; 212:507–511. [PubMed: 20638663]
7. Skarpathiotakis M, Mandell DM, Swartz RH, Tomlinson G, Mikulis DJ. Intracranial atherosclerotic plaque enhancement in patients with ischemic stroke. Am J Neuroradiol. 2013; 34:299–304. [PubMed: 22859280]
8. Dieleman N, van der Kolk AG, Zwanenburg JJM, Harteveld AA, Biessels GJ, Luijten PR, Hendrikse J. Imaging intracranial vessel wall pathology with magnetic resonance imaging: current prospects and future directions. Circulation. 2014; 130:192–201. [PubMed: 25001624]

9. Qiao Y, Steinman DA, Qin Q, Etesami M, Sch€ar M, Astor BC, Wasserman BA. Intracranial arterial wall imaging using three-dimensional high isotropic resolution black blood MRI at 3.0 Tesla. J Magn Reson Imaging. 2011; 34:22–30. [PubMed: 21698704]
10. Qiao Y, Zeiler SR, Mirbagheri S, Leigh R, Urrutia V, Wityk R, Wasserman BA. Intracranial plaque enhancement in patients with cerebrovascular events on high-spatial-resolution MR images. Radiology. 2014; 271:534–542. [PubMed: 24475850]
11. Ryoo S, Cha J, Kim SJ, Choi JW, Ki CS, Kim KH. High-resolution magnetic resonance wall imaging findings of Moyamoya disease. Stroke. 2014; 45:2457–2460. [PubMed: 24947295]
12. Natori T, Sasaki M, Miyoshi M, et al. Evaluating middle cerebral artery atherosclerotic lesions in acute ischemic stroke using magnetic resonance T_1-weighted 3-dimensional vessel wall imaging. J Stroke Cerebrovasc Dis. 2014; 23:706–711. [PubMed: 23871728]
13. Sakurai K, Miura T, Sagisaka T, et al. Evaluation of luminal and vessel wall abnormalities in subacute and other stages of intracranial vertebrobasilar artery dissections using the volume isotropic turbo-spin-echo acquisition (VISTA) sequence: a preliminary study. J Neuroradiol. 2013; 40:19–28. [PubMed: 22633047]
14. van der Kolk AG, Hendrikse J, Brundel M, Biessels GJ, Smit EJ, Visser F, Luijten PR, Zwanenburg JJM. Multi-sequence whole-brain intracranial vessel wall imaging at 7.0 tesla. Eur Radiol. 2013; 23:2996–3004. [PubMed: 23736375]
15. Mugler JP III. Optimized three-dimensional fast-spin-echo MRI. J Magn Reson Imaging. 2014; 39:745–767. [PubMed: 24399498]
16. Park J, Mugler JP, Horger W, Kiefer B. Optimized T_1-weighted contrast for single-slab 3D turbo spin-echo imaging with long echo trains: application to whole-brain imaging. Magn Reson Med. 2007; 58:982–992. [PubMed: 17969106]
17. McCarthy RM, Shea SM, Deshpande VS, Green JD, Pereles FS, Carr JC, Finn JP, Li D. Coronary MR angiography: true FISP imaging improved by prolonging breath holds with preoxygenation in healthy volunteers. Radiology. 2003; 227:283–288. [PubMed: 12616011]
18. van der Kolk AG, Zwanenburg JJM, Brundel M, Biessels GJ, Visser F, Luijten PR, Hendrikse J. Intracranial vessel wall imaging at 7.0-T MRI. Stroke. 2011; 42:2478–2484. [PubMed: 21757674]
19. Wang J, Helle M, Zhou Z, Börnert P, Hatsukami TS, Yuan C. Joint blood and cerebrospinal fluid suppression for intracranial vessel wall MRI. Magn Reson Med. 2016; 75:831–838. [PubMed: 25772551]

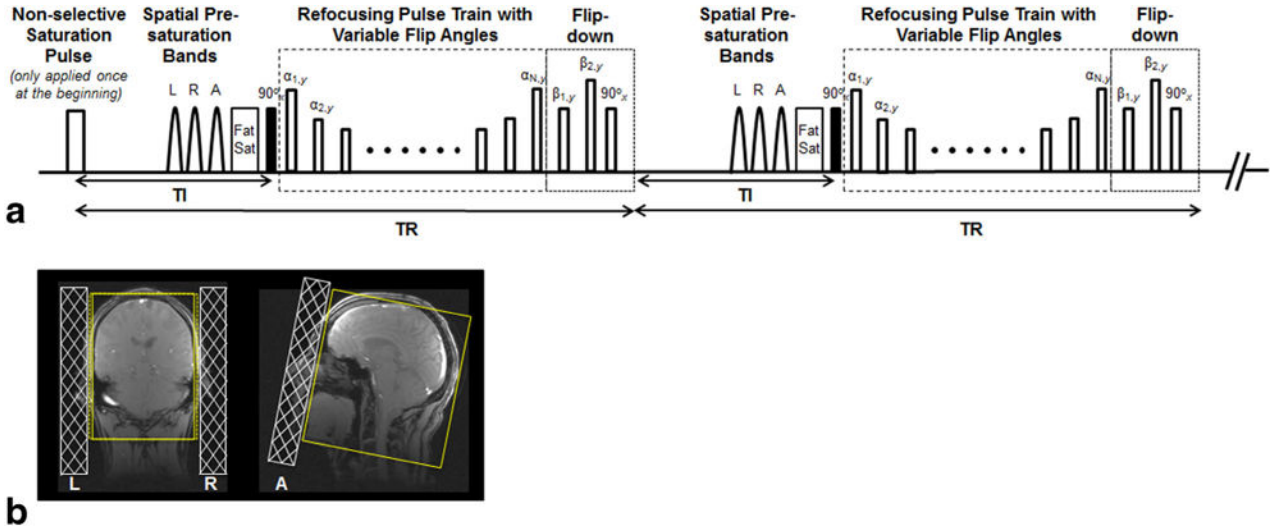

FIG. 1.

(a) Pulse sequence diagram: nonselective saturation pulse is applied only at the beginning to achieve quick transition of magnetizations to a steady state. Three spatial presaturation bands placed on the left (L), right (R), and anterior (A) to saturate the signals from the ears and nose are followed by fat saturation (Fat Sat), nonselective excitation, and a variable-flip-angle refocusing pulse train. A flip-down module is applied immediately after the refocusing pulse train, allowing the remaining magnetizations to be transferred to the *z*-axis, where all tissues subsequently start to undergo inversion recovery. (b) Schematic demonstration of the location of the L, R, and A saturation bands on localization images. These bands help effectively reduce the required phase and partition-encoding steps, and thus minimize scan times.

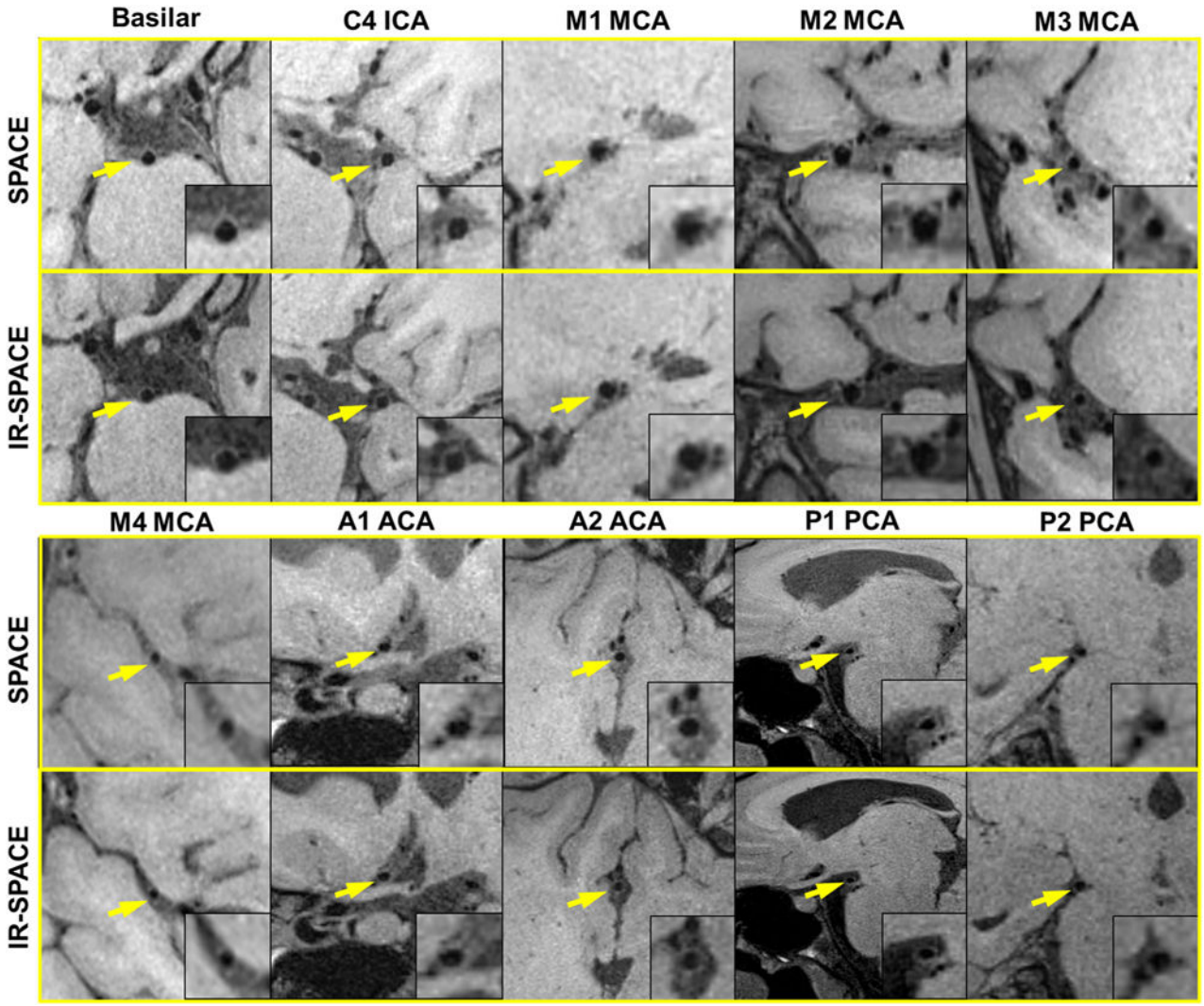

FIG. 2.

Comparison in vessel wall delineation quality between SPACE and IR-SPACE. In a 27-year-old female volunteer, the whole-brain sequence provides exquisite vessel wall depiction of the basilar artery, the supraclinoid (C4) segment of the internal carotid artery (ICA), the M1–M4 segment of the middle cerebral artery (MCA), the A1 and A2 segments of the anterior cerebral artery (ACA), and the P1 and P2 segments of the posterior cerebral artery (PCA). Compared with original SPACE, IR-SPACE offers consistently improved contrast between the vessel wall and surrounding cerebrospinal fluid.

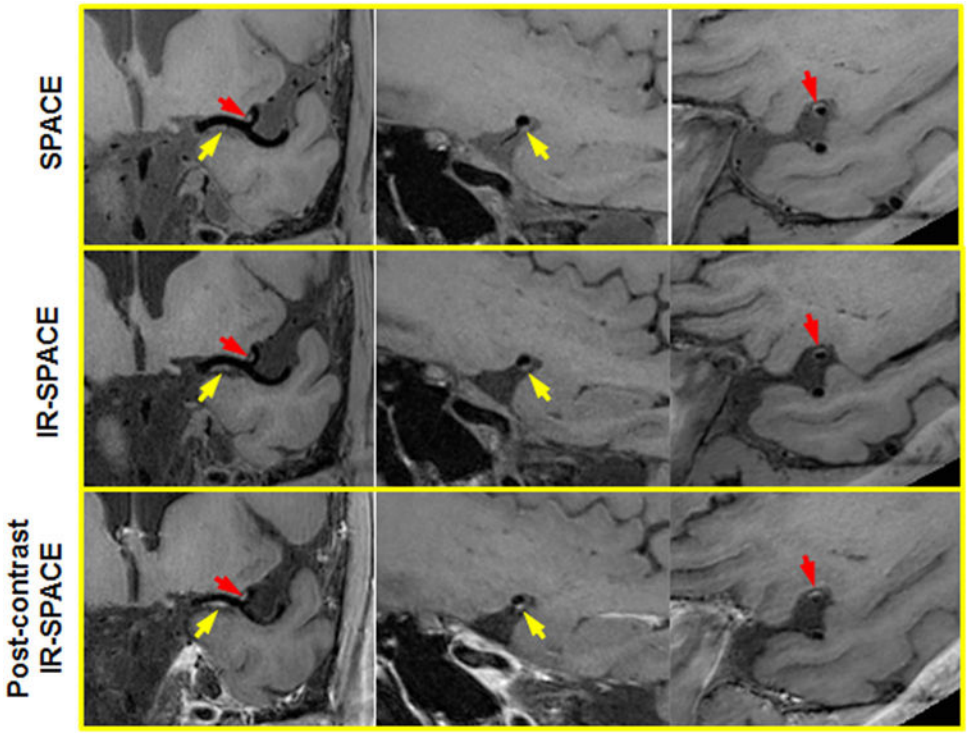

FIG. 3.

A 50-year-old male volunteer with incidental findings. Both SPACE and IR-SPACE in the precontrast state exhibited wall thickening with relatively high signal at the left MCA M1 and M2. Eccentric postcontrast enhancement was also observed at the same locations, indicating atherosclerotic lesions with inflammation. Left column: the in-plane view demonstrating the two suspicious locations (arrows) at MCA M1 and M2, respectively; middle column: the cross-sectional view of the suspicious location at the MCA M1; right column: the cross-sectional view of the suspicious location at the MCA M2.

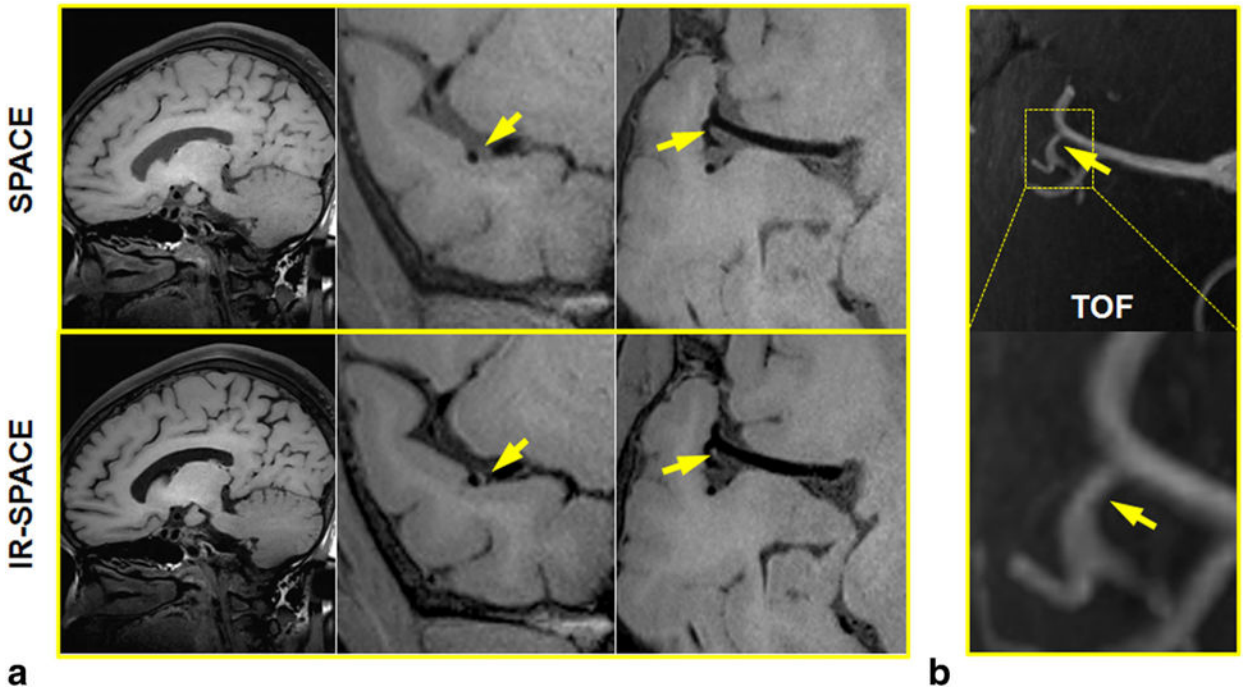

FIG. 4.

A 65-year-old female volunteer with incidental findings. A mild stenosis at the MCA was demonstrated in both SPACE and IR-SPACE. However, wall thickening and relatively high signal at the same location was depicted on IR-SPACE images only as a result of the signal suppression of surrounding cerebrospinal fluid. (a) Left column: sagittal slice demonstrating the overall image quality and contrast weighting; middle and right column: cross-sectional and in-plane views of the M2–M3 trifurcation location showing a mildly stenotic lesion. (b) Time-of-flight thin maximum-intensity-projection images confirming the mild stenosis at the same location.

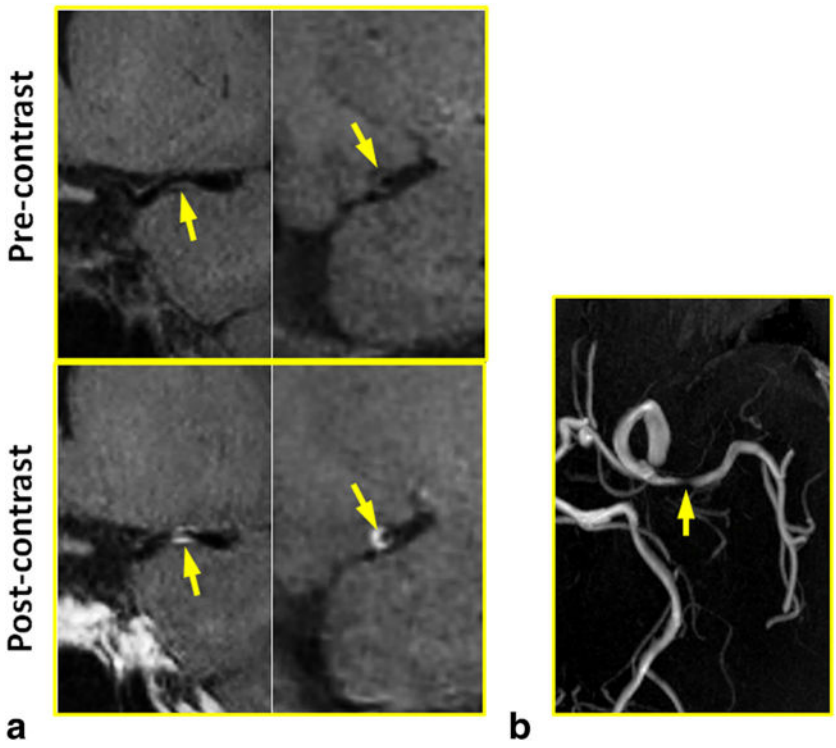

FIG. 5.

In a 57-year-old female patient with atherosclerosis disease, a severe stenosis with eccentric wall thickening and contrast enhancement was detected at MCA by IR-SPACE. Compared with TOF MR angiography, the vessel wall imaging sequence provided more definitive proof that atherosclerosis is involved in the particular part of the vessel wall. (a) Left column: in-plane view demonstrating the stenotic lumen (arrows); right column: cross-sectional view of the atherosclerotic lesion. (b) TOF thin maximum-intensity-projection images confirming the severe stenosis at the same location.

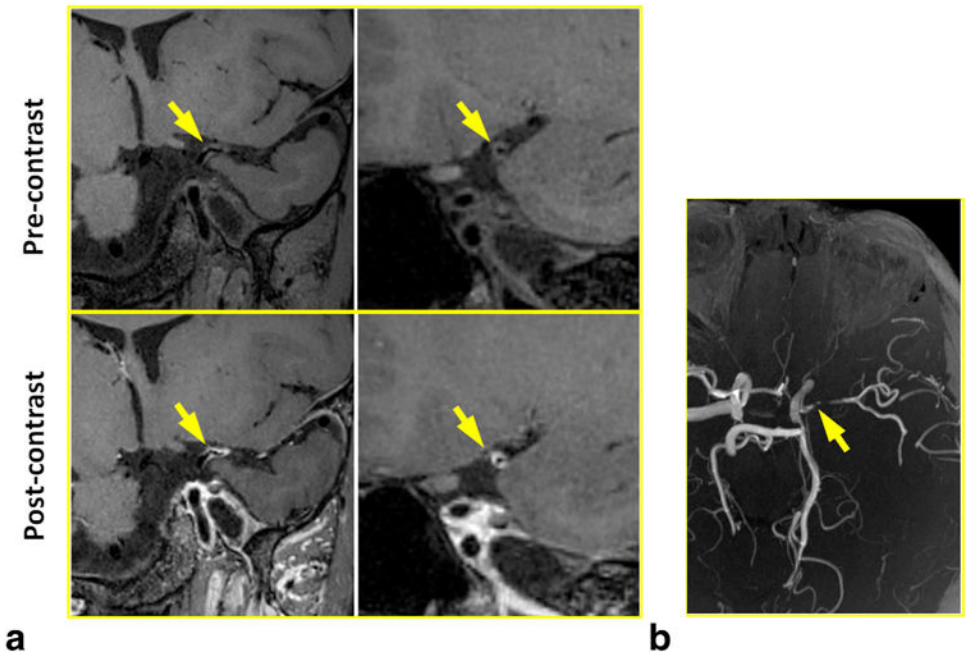

FIG. 6.

In a 37-year-old female patient with lupus disease, severe luminal constriction with concentric wall thickening and contrast enhancement was detected at MCA by IR-SPACE. Compared with TOF MR angiography, the vessel wall imaging sequence provided more definitive proof that inflammation is involved in the particular part of the vessel wall. (a) Left column: in-plane view demonstrating the severely constricted lumen (arrows); right column: cross-sectional view of the lesion. (b) TOF thin maximum-intensity-projection images confirming the severe luminal constriction at the same location.

Table 1

Comparison of Segment-Based Evaluations Between SPACE and IR-SPACE[a]

		All	Basilar	C4 ICA	M1 MCA	M2 MCA	M3 MCA	A1 ACA	A2 ACA	P1 PCA	P2 PCA
Vessel wall delineation	**SPACE**	2.63 (0.49)	3.00 (0.00)	3.00 (0.00)	2.79 (0.39)	2.71 (0.49)	2.64 (0.48)	2.50 (0.50)	2.21 (0.57)	2.57 (0.53)	2.29 (0.49)
	IR-SPACE	2.81 (0.43)	2.86 (0.38)	3.00 (0.00)	3.00 (0.00)	2.93 (0.19)	2.71 (0.49)	2.79 (0.39)	2.43 (0.79)	2.86 (0.38)	2.71 (0.49)
	***P* value**	**0.010**	0.317	1.000	0.180	0.180	0.655	0.194	0.579	0.157	0.083
Sharpness (mm^{-1})	**SPACE**	0.77 (0.52)	1.62 (0.90)	0.94 (0.33)	0.70 (0.29)	0.55 (0.23)	0.57 (0.31)	0.71 (0.29)	0.47 (0.33)	0.74 (0.31)	0.63 (0.39)
	IR-SPACE	1.03 (0.48)	1.63 (0.65)	1.26 (0.44)	1.04 (0.41)	0.91 (0.53)	1.23 (0.61)	0.87 (0.31)	0.74 (0.17)	0.82 (0.26)	0.83 (0.16)
	***P* value**	**<0.001**	**0.946**	**0.041**	**0.035**	**0.038**	**0.033**	0.139	0.074	0.235	0.220

[a]Vessel wall delineation scores (0: ≤ 50% of the vessel wall is visible; 1: > 50% of the vessel wall is visible; 2: the vessel wall is delineated with adequate signal and contrast to the lumen and CSF; and 3: the vessel wall is delineated with excellent SNR and sharp contrast to the lumen and CSF) averaged over the two readers are analyzed using a paired two-tailed Wilcoxon signed rank test. Vessel wall sharpness is analyzed using a paired two-tailed Student's t-test. Statistical significance ($P < 0.05$) is indicated with a bold font. Standard deviations are shown in parentheses.

Note: ICA, internal carotid artery; MCA, middle cerebral artery; ACA, anterior cerebral artery; and PCA, posterior cerebral artery.